AIP | The Journal of Chemical Physics

# New strategy to create ultra-thin surface layer of grafted amphiphilic macromolecules

A. A. Lazutin, E. N. Govorun, V. V. Vasilevskaya, and A. R. Khokhlov

Citation: The Journal of Chemical Physics **142**, 184904 (2015); doi: 10.1063/1.4920973
View online: http://dx.doi.org/10.1063/1.4920973
View Table of Contents: http://scitation.aip.org/content/aip/journal/jcp/142/18?ver=pdfcov
Published by the AIP Publishing

**Articles you may be interested in**

Wetting transitions of polymers via thermal and plasma enhanced atomic layer depositions
J. Vac. Sci. Technol. A **31**, 01A147 (2013); 10.1116/1.4772666

Cyclic olefin copolymer based microfluidic devices for biochip applications: Ultraviolet surface grafting using 2-methacryloyloxyethyl phosphorylcholine
Biomicrofluidics **6**, 012822 (2012); 10.1063/1.3682098

Wetting properties induced in nano-composite POSS-MA polymer films by atomic layer deposited oxides
J. Vac. Sci. Technol. A **30**, 01A105 (2012); 10.1116/1.3639134

Monte Carlo simulations for amphiphilic aggregation near a water phase transition
J. Chem. Phys. **131**, 144901 (2009); 10.1063/1.3244676

Molecular dynamics simulation of amphiphilic molecules in solution: Micelle formation and dynamic coexistence
J. Chem. Phys. **130**, 144901 (2009); 10.1063/1.3105341

How can you **REACH 100%** of researchers at the Top 100 Physical Sciences Universities? (TIMES HIGHER EDUCATION RANKINGS, 2014)
With *The Journal of Chemical Physics*.

AIP | The Journal of Chemical Physics
THERE'S POWER IN NUMBERS. Reach the world with AIP Publishing.

This article is copyrighted as indicated in the article. Reuse of AIP content is subject to the terms at: http://scitation.aip.org/termsconditions. Downloaded to IP: 93.180.55.215 On: Thu, 28 May 2015 10:56:03

THE JOURNAL OF CHEMICAL PHYSICS **142**, 184904 (2015)

# New strategy to create ultra-thin surface layer of grafted amphiphilic macromolecules

A. A. Lazutin,[1] E. N. Govorun,[2] V. V. Vasilevskaya,[1,a)] and A. R. Khokhlov[1,2]
[1]*A. N. Nesmeyanov Institute of Organoelement Compounds RAS, Vavilova ul. 28, Moscow 119991, Russia*
[2]*Faculty of Physics, M. V. Lomonosov Moscow State University, Leninskie Gory, Moscow 119991, Russia*

(Received 27 February 2015; accepted 19 April 2015; published online 14 May 2015)

It was found first that macromolecules made of amphiphilic monomer units could form spontaneously an ultra-thin layer on the surface which the macromolecules are grafted to. The width of such layer is about double size of monomer unit consisting of hydrophilic *A* (repulsive) and hydrophobic (attractive) *B* beads. The hydrophilic *A* beads are connected in a polymer chain while hydrophobic *B* beads are attached to *A* beads of the backbone as side groups. Three characteristic regimes are distinguished. At low grafting density, the macromolecules form ultra-thin micelles of the shape changing with decrease of distance *d* between grafting points as following: circular micelles—prolonged micelles—inverse micelles—homogeneous bilayer. Those micelles have approximately constant height and specific top-down *A-BB-A* structure. At higher grafting density, the micelles start to appear above the single bilayer of amphiphilic macromolecules. The thickness of grafted layer in these cases is different in different regions of grafting surface. Only at rather high density of grafting, the height of macromolecular layer becomes uniform over the whole grafting surface. The study was performed by computer modeling experiments and confirmed in framework of analytical theory. © *2015 AIP Publishing LLC.* [http://dx.doi.org/10.1063/1.4920973]

## I. INTRODUCTION

The polymer brushes (set of macromolecules grafted on a surface) found a numerous practical applications in many important technical fields, such as colloidal stabilization, drug delivery, and biomaterials.[1,2] Depending on the molecular weight of the end-grafted macromolecules and the density of the grafting sites, these polymers are more or less stretched perpendicularly to the grafting surface.[3,4] With a variation of an external stimuli (solvent quality and temperature), polymer brushes could undergo the transition from a homogeneous polymer layer, in which all macromolecules of the layer are extended and are maximally exposed to the solvent (brush mode), to the state in which the chains aggregate into mushroom micelles particularly distributed over the surface (the mushroom-micelle mode). It allows controlling effectively the surface properties; for example, adsorption can be "switched on" and "switched off", and makes the polymer brush to be particularly useful to change promptly the surface properties during operation of the system.

At moderate grafting density, grafted polymers in a poor solvent were studied by numerical methods and the scaling theory was also developed.[5] All approaches predicted the formation of such morphologies as an inverted solvent micelle or hole in the polymer layer, a lamella-like micelle structure, and fused spherical micelle structures. Experimentally, only single end-grafted chains and fused micelles were detected by scanning force microscopy at low and moderate grafting densities;[6] besides, the formation of semi-continuous dimples was observed when end-functionalized polystyrene molecules were adsorbed in poor-solvent conditions.

The diblock copolymer brushes consisting of two *A* and *B* incompatible components exhibit phase separation with the formation of more types of mesophase morphologies.[7–15] Experimental, computer-aided, and theoretical studies showed that mesophase ordering depends on the surface grafting density of the polymer chains, the relative length of each of the blocks and the energy of *A* and *B* interaction with the solvent and with each other. In case of compatible *A* and *B* components in poor solvent at relatively low grafting density, the resulting structures have a core of less soluble blocks, the shape of which is determined by the block length ratio. Two types of structures were distinguished in Ref. 16: the micelles in which the spherical core of the less soluble block is enveloped by the spherical shell of a more soluble block (the authors called them onion-like micelles) and the micelles composed of a few cores uniformly enveloped by a layer of a more soluble block (they were referred to as garlic-like micelles). In case of the solvent which is poor for the block directly grafted to the surface and is good for the outer block, the resulting micelles have a "flowerlike" structure composed of a few chains with a hydrophobic core and hydrophilic petals exposed to the solvent.[17]

If one of the blocks possesses a preferential interaction with the solvent, the brush self-assembles so that the more soluble block is in a greater contact with the solvent.[18] If the solvent is good for the inner block (grafted onto the surface) and poor for the outside block, the inner blocks are exposed to the solvent and the outside blocks form a structure whose morphology depends on the grafting density and block length. Calculations showed that, as the grafting density and length of

a)Author to whom correspondence should be addressed. Electronic mail: vvvas@polly.phys.msu.ru

 © 2015 AIP Publishing LLC

This article is copyrighted as indicated in the article. Reuse of AIP content is subject to the terms at: http://scitation.aip.org/termsconditions. Downloaded to IP: 93.180.55.215 On: Thu, 28 May 2015 10:56:03

macromolecules increase, one can observe a series of transition: spherical micelle–stripes–perforated lamella–continuous layer of outer block on the surface of the film.[19–21]

In dense copolymer brushes with incompatible *A* and *B* blocks,[22,23] layering phase separation could be observed: a structure of three layers with different concentrations of monomer units *A* and *B* is formed. In the case of strong *AB* incompatibility, the blocks are almost completely separated and a well-defined thin interface between the inner and outer block appears. The outer blocks are "grafted" on this interface with the randomly distributed grafting points which "move" effectively along the surface.[24] In nonselective solvents, the dense *AB* brushes could form various perpendicularly oriented domains called "golf holes", "gullies", "ridges", and "stalactites".[25]

Self-assembly in homopolymer brushes with the formation of strands perpendicular to the grafting surface is predicted theoretically for the case of dimer solvent molecules (surfactant).[26] The difference in the interaction energies of two parts of surfactant molecule with polymers leads to the possibility of spatial separation of polymer and surfactant in the brush.

In this paper, we consider self-organization of brush of macromolecules being amphiphilic on the level of individual monomer units, in the meaning that each monomer unit contains both hydrophobic and hydrophilic groups. The duality of the monomer units results in their simultaneous affinity and incompatibility with both polar and organic solvents. In a mixture of incompatible hydrophobic and hydrophilic solvents, such monomer units prefer to be located at the interface rather than in the bulk of one of the solvents.[27–29] The classification of monomer units with respect to this feature was introduced in Refs. 28 and 29, and a simple model was suggested in Ref. 30, where individual monomer units were considered to be dumbbells consisting of hydrophobic *H* and hydrophilic *P* beads, linked by a fixed-length bond.

Computer simulations showed that amphiphilicity at the level of individual monomer units leads to dramatic complication and enrichment of the set of possible conformational transitions, compared to that of ordinary homopolymer macromolecules.[30–35] The globules of such macromolecules have a complex core-shell structure: the interiors consist of hydrophobic units, while the outer shell is composed of hydrophilic units. In semidilute solution, the amphiphilic flexible macromolecules condense into individual soluble globules[31] while the rigid macromolecules tend to aggregate with formation of braid fibril-like complexes[36] or bundle aggregates of a few chains.[37] In both cases, the hydrophobic backbones of the chains intertwine and form a core, whereas hydrophilic groups are located on the surface. The hydrophilic shell prevents the bundle aggregation and favors the parallel location of the bundles in concentrated solution.[37] The phase diagram for the melt of copolymers with an amphiphilic block can be significantly different from that known for the conventional diblocks.[38,39] In the limit of significant amphiphilicity (surface activity), the resulting morphology corresponds to thin channels and slits of amphiphilic units penetrating through the matrix of a majority non-polar component. The voids are found to concentrate on the interfaces and to perform crystalline-like ordering in case of significant amphiphilicity of units.[40]

The theoretical study[41,42] of morphological states of macromolecules with amphiphilic monomer units shows that the crucial factor stabilizing the shape of macromolecules in a condensed globular state is the surface tension decrease due to the polar group orientation towards the external solution.

It is worthwhile to propose that the high surface activity of monomer units could favor the specific phase ordering in the polymer brushes. This paper addresses the self-organization of polymer brushes with amphiphilic monomer units as function of solvent quality and grafting density. The further presentation is organized as follows. Section II, the model of the neutral polymer brush with an amphiphilic monomer units and molecular dynamic simulation routine are described. In Sec. III the results of simulation are listed and discussed. Section IV presents a theoretical model and data. In the Conclusion, results are summarized.

## II. THE MODEL AND SIMULATION TECHNIQUE

We consider polymer brush of amphiphilic macromolecules grafted onto a flat surface. According to the main objective of the study, the macromolecule is comprised of amphiphilic monomer units represented as "dumbbells" consisting of two beads: a solvophilic *A* unit and a solvophobic *B* unit. The dumbbells form an *AB* polymer with a backbone of *N* solvophilic *A* beads connected in a linear fashion and *N* solvophobic *B* beads attached to the backbone, as shown in Figure 1.

The polymer layer examined in this study is composed of *m* macromolecules with length *N* grafted at regular intervals onto a planar impermeable surface XY at the sites of a square lattice with edge $d$. The grafting density is $1/d^2$, where $d^2$ is the area per macromolecule. The polymer layer is immersed in a bath with selective solvent which is poor for *B* beads and good for *A* beads.

In the numerical simulations, we adapted a continuum space model. The temporal evolution of the system was found by solving a system of Newton equations via the molecular dynamics (MD) technique with the LAMMPS software package.[43] We used the simulation resources of the Supercomputing Center of Lomonosov Moscow State University.[44]

In MD simulation, the excluded volume between any two beads is interpreted in terms of a repulsion potential of the

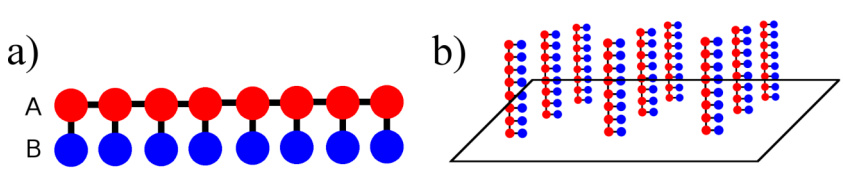


FIG. 1. Cartoons of the amphiphilic macromolecules (a) and grafted layer of such macromolecules (b).

This article is copyrighted as indicated in the article. Reuse of AIP content is subject to the terms at: http://scitation.aip.org/termsconditions. Downloaded to IP: 93.180.55.215 On: Thu, 28 May 2015 10:56:03

Lennard-Jones type,

$$u_S(r_{ij}) = \begin{cases} 4\varepsilon\left[\left(\frac{\sigma}{r_{ij}}\right)^{12} - \left(\frac{\sigma}{r_{ij}}\right)^{6} + \frac{1}{4}\right], & r_{ij} \le r_c \\ 0, & r_{ij} > r_c \end{cases}, \quad (1)$$

where $r_{ij}$ is the distance between the $i$th and $j$th monomer units, $r_c = \sqrt[1/6]{2}\sigma$ is the cut-off distance. The parameter $\varepsilon$ governs the strength of interaction and controls an energy scale, whereas $\sigma$ defines a length scale. We assume that $\sigma = \varepsilon = 1$ for all interactions. All of our results are therefore reported in terms of these natural units.

For simplicity, we assume that there is no interaction between $A$ units except that corresponding to excluded-volume potential (1). The hydrophobic interaction of side-beads $B$ is modeled by a Yukawa-type potential,

$$u_{\mathrm{BB}}(r_{ij}) = \begin{cases} \varepsilon_{BB}\left[\frac{\exp(-\kappa r_{ij})}{r_{ij}} - \frac{\exp(-\kappa r_{cut})}{r_{cut}}\right], & r_{ij} < r_{cut} \\ 0, & r_{ij} \ge r_{cut} \end{cases}. \quad (2)$$

In this equation, $r_{cut}$ is the cut-off distance ($r_{cut} = 4\sigma$), $\kappa = 1.2$ is the inverse screening length, and $\varepsilon_{BB}$ denotes the characteristic energy of $B$–$B$ interactions. The characteristic energy $\varepsilon_{BB}$ is negative and varies in course of experiment ($\varepsilon_{BB} < 0$). It must be emphasized that the potential (2) is, of course, only a prototype of a realistic potential. However, numerous computer modeling of polymer systems shows that the equilibrium properties of macromolecular systems do not depend on the exact form of the potentials but depend on well depth $\varepsilon_{BB}$ and radius of interaction $r_{cut}$.

The decrease of energetic parameter $\varepsilon_{BB}$ (increase of attractive interaction between side groups $B$) induces effective worsening of solvent quality.

The solvent quality was characterized by $\chi$ parameter being combination of second virial coefficients of paired $A$-$A$, $A$-$B$, and $B$-$B$ interactions,[45,46]

$$\chi = 1/\upsilon\left(v_2^{AB} - \frac{v_2^{AA} + v_2^{BB}(\varepsilon_{BB})}{2}\right), \quad (3)$$

where $\upsilon$ is the effective volume of monomer unit, and $v_2^{AA}$, $v_2^{AB}$, $v_2^{BB}(\varepsilon_{BB})$ are second virial coefficients which are calculated as

$$v_2^{Ai} = \int_0^{r_{cut}} \left[1 - \exp(-\frac{u_s(r)}{k_B T})\right] dr^3, \quad i = A, B \quad (4)$$

$$v_2^{BB}(\varepsilon_{BB}) = \int_0^{r_{cut}} \left[1 - \exp(-\frac{u_s(r) + u_{BB}(r)}{k_B T})\right] dr^3. \quad (5)$$

In the case under consideration, $\upsilon \equiv v_2^{AA} = v_2^{AB} \sim 2.14$. The $\chi$ parameter represents the kind of interactions parameter used in simple lattice systems such as in Flory-Huggins theory[45,46] and characterizes solvent quality in an integral manner.

The bonds within a given macromolecule are constrained via a finite extensible nonlinear elastic (FENE) potential,[47]

$$E_{FENE}(r) = -\frac{K}{2}R_0^2 \ln\left[1 - \left(\frac{r}{R_0}\right)^2\right], \quad (6)$$

where $r$ is the distance between connected beads, $K = 30$ is a coefficient that reflects the rigidity of the bond, $R_0 = 1.5$ is the maximum bond length. An equilibrium bond length $a$ is determined by interplay of elastic (6) and excluded volume (1) interactions. It is found that $a$ is approximately equal to $a = 1.2$, and for the characteristic ratio $\upsilon/a^3$, we have the following estimation: $\upsilon/a^3 \approx 1.24$.

The impermeability of the surface was described as a steric interaction between beads and surface via a truncated 9-3 Lennard-Jones potential,[48]

$$E_s(r) = \begin{cases} \varepsilon_s\left[\frac{2}{15}\left(\frac{\sigma}{r}\right)^9 - \left(\frac{\sigma}{r}\right)^3 + \sqrt{\frac{10}{9}}\right], & r < r_{cut} \\ 0, & r \ge r_{cut} \end{cases}, \quad (7)$$

where $r$ is distance between monomer units and surface, $\varepsilon_s$ is a parameter that characterizes the energy of interaction, $r_{cut} = \sqrt[6]{2/5}\sigma$ is cut-off distance. In our calculation, we propose that the parameter $\varepsilon_s$ is the same for $A$ and $B$ beads and is equal to $\varepsilon_s = 2\varepsilon$.

To take into account the fact that the system is in contact with a thermostat at temperature $T$ ($T = \varepsilon/k_B$, where $k_B$ is the Boltzmann constant), the motion equations were supplemented with a term that described friction and the Langevin uncorrelated noise term $R_i$, which is related to the viscosity of the solvent through the fluctuation dissipation theorem,[49]

$$\langle R_{\alpha i}(0) \cdot R_{\alpha i}(t)\rangle = 2\Gamma k_B T \delta(t), \quad (8)$$

where $\delta(t)$ is the Dirac delta function; $\alpha = x, y, z$ coordinates, $i = 1, \ldots, \boldsymbol{M}$; and $\boldsymbol{M}$ is the total number of particles. Parameter $\Gamma$ is equal to 0.01 in all calculations.

The computations were performed for macromolecules composed of $N = 32$ monomer units. The distance between grafting points $d$ was varied from $d = 2$ till $d = 20$. The values $d$ are expressed in σ units (Eq. (1)) which relate to the bond length as $a = 1.2\sigma$. The total number of grafted macromolecules in all experiments performed was equal to $m = 400$. The protocol for the simulation was as follows. In the initial configuration, the polymer chains were put on the XY plane at the sites of a square lattice with the edge $d$ and then extended in the direction of the $z$ axis (Fig. 1(b)). The Flory-Huggins interaction parameter $\chi$ was varied from 0.57 to 5.7 with a step $\Delta\chi = 0.2$. At $\chi = 0.57$ (ideal solvent) the chains were uniformly distributed over the cell; with an increase in the energy $\varepsilon$, they aggregated into clusters. At each value of $\chi$ parameter, the computation was performed for $2 \times 10^6$ integration steps. Within the first $1 \times 10^6$ steps, the system underwent equilibration. The selected duration of initial computations was sufficient for the relaxation of the system to the equilibrium, i.e., non-dependent on time, mean values of total energy, radius of gyration of macromolecules, and other calculated characteristics. During the rest of the simulation time ($1 \times 10^6$), the observed values were averaged to obtain their mean values and mean-square deviation. For each set of parameters $a$ and $\chi$, we performed visual analysis

This article is copyrighted as indicated in the article. Reuse of AIP content is subject to the terms at: http://scitation.aip.org/termsconditions. Downloaded to IP: 93.180.55.215 On: Thu, 28 May 2015 10:56:03

and determined the distributions of aggregates with respect to the number of chains contained in them $M$, the mean aggregation number $\langle M \rangle$, the distribution $\rho_i$ ($i = A, B$) of $A$ and $B$ beads over distance $z$ to the grafting plane, also the fraction $f_S$ of surface being covered by polymer was estimated and surface relief was constructed.

## III. RESULTS

Depending on the density of grafting of macromolecules, we had distinguished three characteristic regimes: regime of ultra-thin micelles at low grafting $d \geq d_0$, of over-built bilayer micelles at dense grafting at $d^* \leq d < d_0$, and of super dense grafting at $d < d^*$. The monomer units, spreading homogeneously over grafting surface, form the thin bilayer of monomer units at $d = d_0$ and the double bilayer at $d = d^*$. The values $d^*$ and $d_0$ are determined exclusively by macromolecular parameters, the size of monomer unit, and the degree of polymerization. The distances $d_0$ and $d^*$ are related with each other as $d^* \sim d_0/\sqrt{2}$.

Let us start from the case of low grafting density $d \leq d_0$. Figure 2 shows the snapshots of the simulation cell at different solvent quality $\chi$. At relatively good solvent ($\chi = 0.57$), the polymer chains form homogeneous layer on the surface (Figure 2(a)). Worsening solvent quality (increase of $\chi$) leads to the aggregation of macromolecules into clusters (Figure 2(b)). In poor solvent, the macromolecules form micelles (Figures 2(c) and 2(d)). The aggregates have a flattened shape of "spiders" with protruding "legs," or parts of individual chains, which extend from the grafting points to the micelle core (Figures 2(c) and 2(d)). One can see that with worsening solvent quality the "spider body" becomes narrow and spread over the surface. The micelle core in poor solvent could be considered as bilayer with inner part composed of attractive $B$ beads. $A$ beads are situated on the surface below and above $BB$ layer. The micelle core thickness is approximately twice the size of amphiphilic monomer units which was confirmed quantitatively by calculations of the distribution of beads $A$ and $B$ over distance $z$ from grafting surface (results are shown and discussed below).

To characterize the aggregation process quantitatively, we have calculated the aggregation number $M$ and fraction $f_S$ of covered surface.

The aggregation number $M$ was defined as a number of macromolecules belonging to the cluster. Two macromolecules are part of the cluster if at least two beads of different macromolecules are on a distance less than 1.5. The aggregation number $M$ was averaged over the cell and over different realizations. The dependences of average aggregation number $\langle M \rangle$ on solvent quality $\chi$ are shown in Figure 3. One can see that the aggregation number $\langle M \rangle$ increases with the increase of grafting density both in good and in poor solvent.

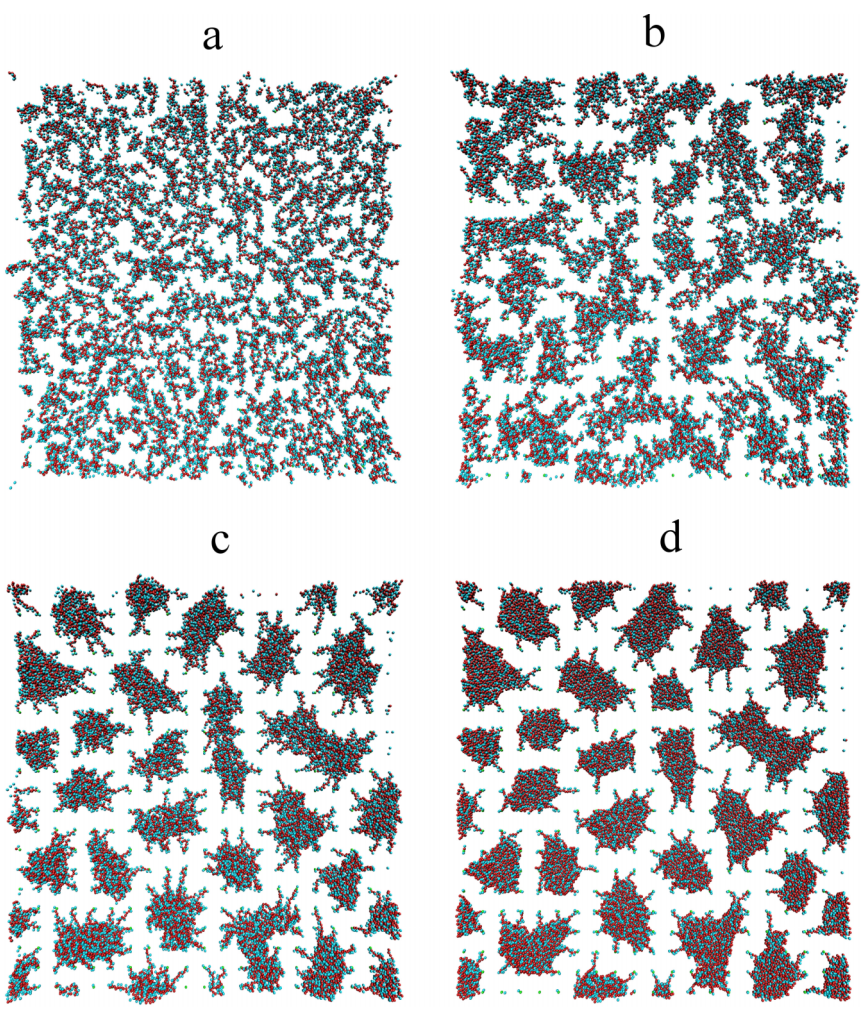


FIG. 2. Snapshots of cells ($d = 7$) at different solvent qualities parameter $\chi$: 0.57 (a), 1.89 (b), 3.09 (c), 5.7 (d). The main chain beads are shown in red and the side beads are blue. The grafting points are colored in green.

This article is copyrighted as indicated in the article. Reuse of AIP content is subject to the terms at: http://scitation.aip.org/termsconditions. Downloaded to IP: 93.180.55.215 On: Thu, 28 May 2015 10:56:03

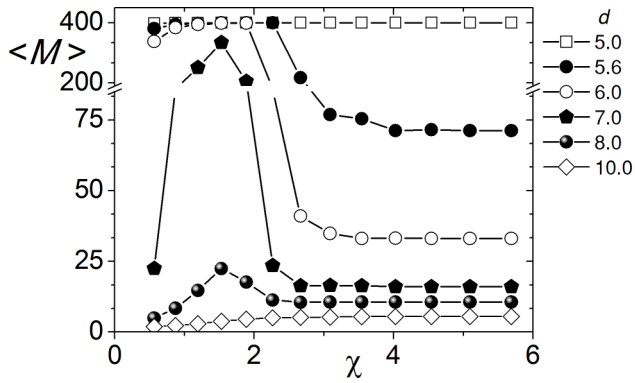


FIG. 3. Dependences of the average aggregation number $\langle M \rangle$ on solvent quality $\chi$ for different distances $d$ between grafting points.

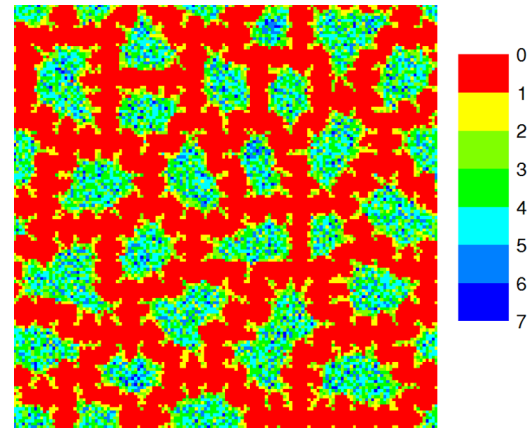


FIG. 4. The map of surface density $\rho_s$ for $\chi = 5.7$ and $d = 7$.

$\langle M \rangle$ grows with worsening of solvent quality monotonically in case of low ($d > 10$) and high ($d < 5$) grafting density. In intermediate case ($5 < d < 10$), the average aggregation number $\langle M \rangle$ is a non-monotonic function of solvent quality $\chi$. In good solvent, the macromolecules are swollen and the aggregation number here shows number of random contacts between different macromolecules. Weak attractive interactions favor the contacts between attractive $B$ beads but macromolecules are still swollen and number of contact between different macromolecules and so far the aggregation number $\langle M \rangle$ increases (Figure 2(a)). Further increase of $\chi$ leads to the compaction of macromolecules, formation of dense aggregates and drop of the average aggregation number $\langle M \rangle$. The change in $\langle M \rangle$ value could be significant. In case of $d = 7$, the aggregation number $\langle M \rangle$ changes from $\langle M \rangle \sim 25$ at $\chi \sim 0.5$ to $\langle M \rangle \sim 350$ at $\chi \sim 1.7$ and till $\langle M \rangle \sim 20$ at $\chi > 2.5$.

To calculate the fraction $f_S$ of covered surface, we first create the map of surface density $\rho_s$ of beads. Towards this end, the grafting surface was divided into sites and the number of monomer beads in each site was calculated. It was proposed that the bead belongs to the given site if $XY$ projection of its center of mass is found to be within this site. The size of site was optimized so that the beads of aggregate body and "legs" could be differentiated.

An example of local density map for $\chi = 5.7$ and $d = 7$ is presented in Figure 4. The sites were colored in different colors in accordance with the site density. A color scale is shown as a legend on the right.

In the case shown in Figure 4, the surface density of legs and the surface density of micelle border are $\rho_s$ = 1-2 (shown by yellow and light green). The surface density of aggregates body is mainly within the interval from $\rho_s = 3$ to $\rho_s = 4$ (dark green and light blue). However, within the aggregate body, some fraction of sites have density up to $\rho_s = 6$ (dark blue), and few sites have density as low as $\rho_s = 1$ (yellow) due to the discrete representation of the surface. To differentiate sites with low density belonging to inner parts of micelles from those lying on micelle borders or belonging to "legs," the following adapted technique was used. The sites with density $\rho_s \geq 3$ are considered as belonging to the micelle body. The sites with density $\rho_s = 1$ or 2 are referred to the micelle body (if at least 5 of 9 adjacent sites have density $\rho_s \geq 3$), to the micelle border (if from 1 to 4 adjacent sites have density $\rho_s \geq 3$), or "leg" (if the density in all adjacent sites is lower than 3). The fraction of covered surface, $f_S$, is determined as an area ratio of the micelle body plus border sites and the grafting plane.

The dependences of fraction $f_S$ of covered grafting surface on solvent quality $\chi$ are shown in Figure 5. One can see that $f_S$ is a non monotonic function: the formation of aggregates first leads to the compaction of macromolecules and increase of empty fields on grafted surface ($f_S$ decreases). Then due to the amphiphilicity of monomer units, the aggregates become thinner and cover larger part of grafted surface (compare Figures 2(c) and 2(d)).

In poor solvent, the increase of grafting density leads to increase of aggregation number $\langle M \rangle$ and thus to increase of fraction $f_S$ of surface which is covered by aggregates. Similarly to the homogeneous brush,[5] depending on the grafting density $1/d^2$ in poor solvent, the macromolecules could form the spherical micelles, the elongated micelles, inverted micelles, and homogeneous layer (Figure 6). One can see that the distribution of micelles over aggregation number $M$ could be rather wide and that the micelles of different shape could coexist. Analysis shows that in all the cases for $d_0 = 4.2 < d < 12$, the dense parts of aggregates are nothing but a thin *A-BB-A* bilayer of macromolecules spread close the grafting surface.

The dependences of the average aggregation number $\langle M \rangle$ and fraction $f_S$ of covered surface on $d$ are shown in

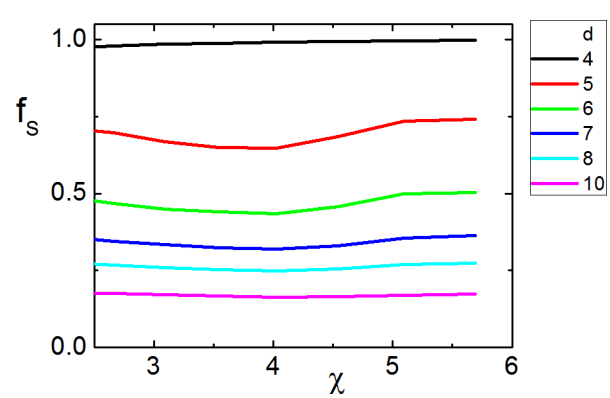


FIG. 5. The covered fraction $f_S$ of grafting surface as a function of solvent quality $\chi$ for different grafting densities.

This article is copyrighted as indicated in the article. Reuse of AIP content is subject to the terms at: http://scitation.aip.org/termsconditions. Downloaded to IP: 93.180.55.215 On: Thu, 28 May 2015 10:56:03

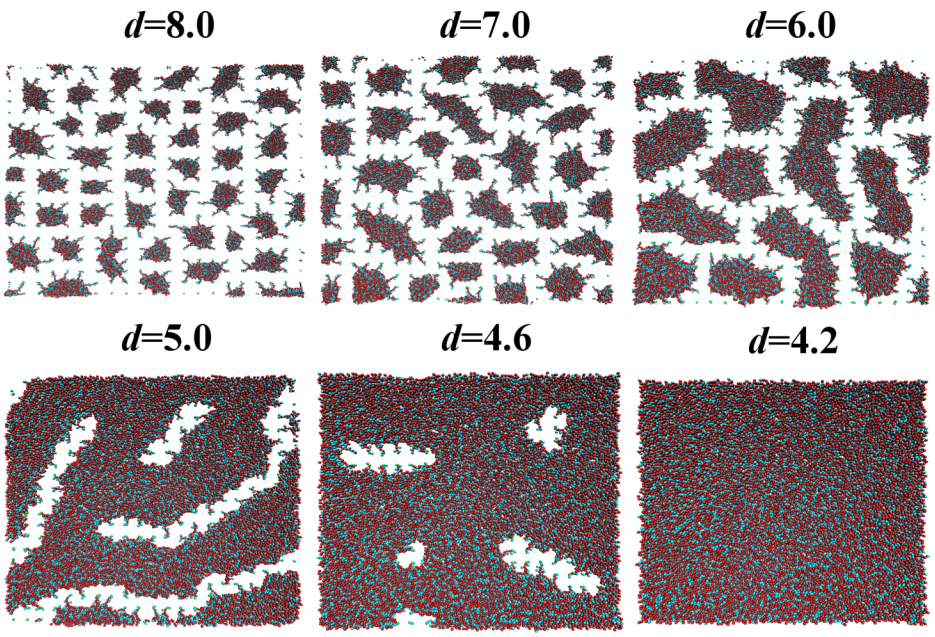


FIG. 6. Snapshots of cells with different distance between grafting points $d$ at $\chi = 5.7$.

Figure 7. One can see that the average aggregation number $\langle M \rangle$ increases with decrease of distance $d$ between grafting point and at $d = 5.2$ all macromolecules are joined into the single cluster. This point could be considered roughly as transition from elongated micelles to inverted micelles (see Figure 6, $d = 6$ and $d = 5$). The fraction $f_s$ of covered surface increases with growth of grafting density as well. It scales approximately as $f_S \sim 1/d^2$ and goes to plateau at $d_0 \sim 4.2$ when collapsed macromolecules cover all grafting surface (Figure 6, $d = 4.2$).

Generally speaking, for $d > d_0$ one can distinguish two types of macromolecules: macromolecules forming legs and so-called spider body macromolecules. In our calculation, we propose that macromolecule belongs to spider body if its grafting point is under the cluster otherwise the macromolecule is partly a "spider leg". Figure 8 shows the dependence of fraction $K_{gr}$ of "spider body" macromolecules on the distance $d$ between grafting points. This dependence is not monotonic: at high values of $d$ ($d > 20$) macromolecules mainly form separated globules with grafting points under compacted near spherical globule and $K_{gr} = 1$. At $12 < d < 20$, the single macromolecule clusters with $K_{gr} = 1$ coexist with few macromolecules clusters which have legs and $K_{gr} < 1$. $K_{gr}$ decreases till $K_{gr} = K_{gr}^{min}$ at $d \sim 12$ where the aggregation number of all clusters becomes higher than unity. The further decrease of $d$ leads to the further increase of aggregation number of clusters, expansion of covered surface and growth of $K_{gr}$. At $d \leq d_0 = 4.2$, the total grafting surface is covered by aggregates and $K_{gr}$ become equal to unity $K_{gr} = 1$.

Figure 9 shows the distributions $\rho_A$ of $A$ and $\rho_B$ of $B$ beads over distance $z$ from grafting surface for different distances $d$ between grafting points at poor solvent with $\chi = 5.7$. The distributions $\rho_B$ for side groups $B$ are shown by thin lines, the distributions $\rho_A$ for main-chain $A$ groups are drawn by thick lines. The distance $z$ from the grafting surface is normalized by bond length $a$. The cases of relatively low grafting density $d > d_0 = 4.2$ are shown in Figure 9(a), the distributions for densely grafted systems ($d < d_0$) are given in Figure 9(b). One can see that for $d > d_0$, the aggregates are rather thin: the maximum values of $z$ is less than $5a$. $A$ and $B$ beads are effectively segregated. The side-chain beads $B$ form inner part of clusters while the main-chain beads $A$ are situated on the both side of $BB$ layer.

At $d < d_0 = 4.2$, the width of grafted layer, estimated by the maximum value on the z axis, increases visibly with decrease of distance $d$ between grafting points (Figure 9(b)). The $A$ and $B$ beads are effectively separated in this case as well. In all the cases, there are two maxima on the distribution $\rho_A(z)$ nearby the grafting surface and on the distance $4a$ from it. The distributions $\rho_B(z)$ have maximum with double peaks between two maxima on the $\rho_A(z)$ plots. Thus, $A$-$BB$-$A$ layer nearby the grafting surface in all the cases is formed.

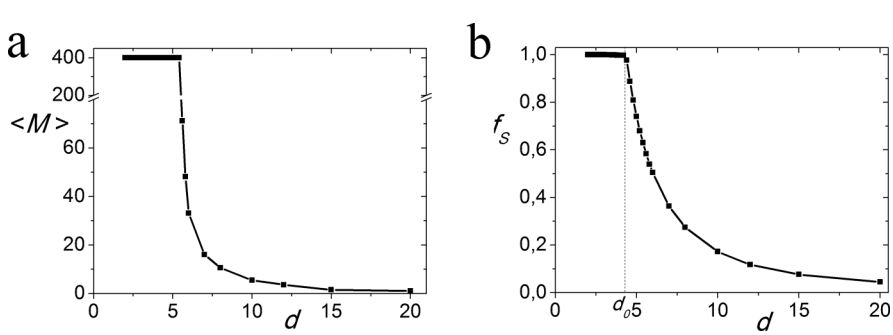


FIG. 7. Average aggregation number $\langle M \rangle$ (a) and fraction $f_S$ of covered surface (b) as function of distance $d$ between grafting point at $\chi = 5.7$.

This article is copyrighted as indicated in the article. Reuse of AIP content is subject to the terms at: http://scitation.aip.org/termsconditions. Downloaded to IP: 93.180.55.215 On: Thu, 28 May 2015 10:56:03

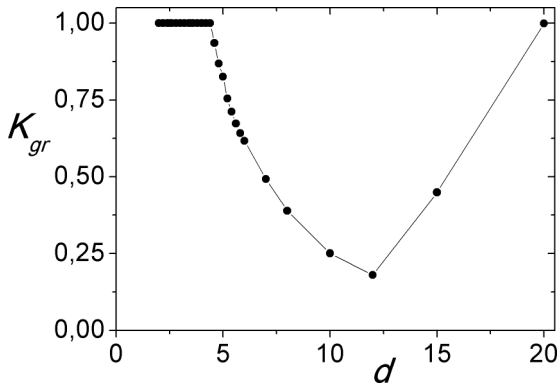


FIG. 8. Fraction $K_{gr}$ as function of distance $d$ between grafting points at $\chi = 5.7$. Comments are given in the text.

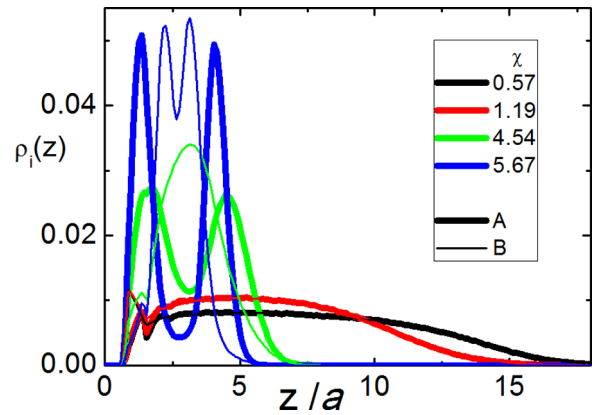


FIG. 10. Distributions $\rho_A$ of $A$ (thick line) and $\rho_B$ of $B$ (thin line) beads over the distance $z$ from the grafting surface for different $\chi$ at $d = d_0 = 4.2$.

Figure 10 presents the distributions $\rho_A(z)$ and $\rho_B(z)$ for different solvent quality at $d = 4.2$. One can see that in good solvent, the distributions $\rho_A(z)$ of main chain $A$ and $\rho_B(z)$ of side $B$ groups coincide and polymer layer is homogeneous with respect to $A$ and $B$ distributions. As solvent quality become poorer, the thickness of layer decreases. Then, $A$ and $B$ beads separate: $B$ beads go to the inner part while $A$ beads cover them from both sides. In poor solvent ($\chi > 5$), the $B$ beads are densely packed: the distribution $\rho_B(z)$ represents the double peaks.

Analysis shows that in case of high density, $d < d_o$, the polymer layers have different thickness in different parts. Figure 11 shows the surface relief of cells for different values of $d < d_0$. To construct the surface relief we colored outer beads, i.e., the beads which are on the outer surface of polymer layer, with respect to their distance from the grafting surface. The bright red corresponds to the lowest distance, bright blue corresponds to highest distance and both colors dim up to white color at intermediate distances. In other words, the surface relief allows to estimate the thickness of layer: the thin parts are colored in bright red and the most thick parts of compacted polymer layer are shown by bright blue. One can easily distinguish the regions with different thickness of polymer layer on surface relief (Figure 11). Analysis shows that the thickness of red parts is about 4a which corresponds to the thickness of (*A-BB-A*) bilayer, the thickness of blue parts is twice more and equal to 8a. On dependence of distance $d$ between grafting points the blue, thick, regions of polymer film could look like spherical and prolonged micelles, some sort of lamellae and inversed micelles. In fact, with increase of grafting density, the shape of blue regions is changed somewhat similar to change of shape of micelles formed at low grafting density at $d > d_0$. Thus, one can conclude that structured micelles are build over the bilayer surface. The double (*A-BB-A*) bilayer covers whole grafting surface at $d^* \sim 3.2$.

The results are confirmed by visual analysis of side views of simulation cell (Figure 12). One can distinguish bilayer structure with micelles on its top for $d = 3.2$-$3.8$. It could look as a double bilayer structure *A-BB-A-BB-A* in some places. Analysis shows that at $d \sim 3$ one can observe double bilayer over the whole surface. It could be treated as a boundary value $d^*$ between over-build micelle regime and that of super dense grafting. It is clear that since the surface grafting density ($\sim 1/d^2$) at $d^*$ is twice the grafting density at $d_0$, the following relation between $d^*$ and $d_0$ is valid: $d^* = d_0/\sqrt{2}$. The parallel to grafting surface ordering is lost in case of super densely grafting cases ($d < 3$). It seems that some sort of microscopic separation with vertically oriented phases exists in super densely grafted layer ($d < d^*$). To understand type of self-assembly in the case of such super dense grafting, it is necessary to made calculations for longer macromolecules. We are going to perform such type of calculations in forthcoming papers.

## IV. THE SCALING THEORY

To analyze the reasons for the self-assembly of amphiphilic macromolecules on the grafting surface with the formation of various morphologies, the scaling theory arguments can be used. We consider not very high grafting densities ($d \geq d_0$), so that the monomer unit bilayer *A-BB-A* does not cover the

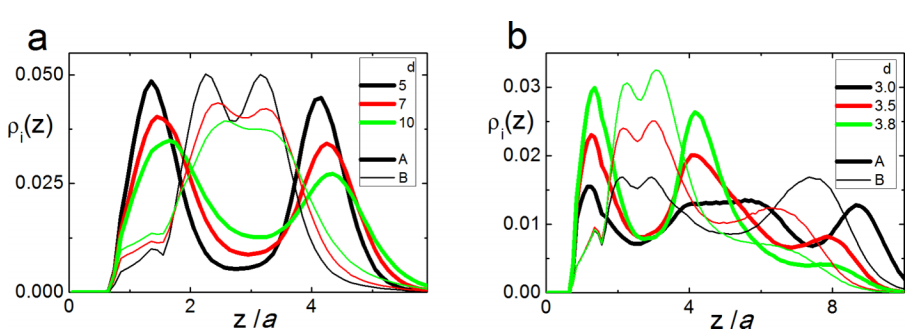


FIG. 9. The distributions $\rho_A$ of $A$ (thick line) and $\rho_B$ of $B$ (thin line) beads over distance $z$ from the grafting surface for different $d$ in regime of ultra-thin micelles ($d > d_0$, a) and regime of over-built bilayer micelles ($d < d_0$, b).

This article is copyrighted as indicated in the article. Reuse of AIP content is subject to the terms at: http://scitation.aip.org/termsconditions. Downloaded to IP: 93.180.55.215 On: Thu, 28 May 2015 10:56:03

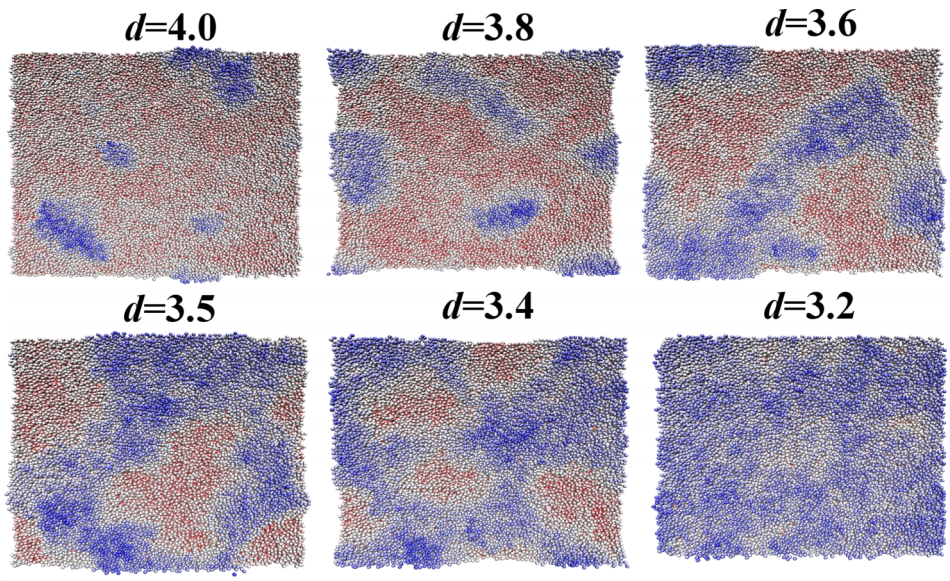


FIG. 11. The surface relief of cells for different values of $d^* < d < d_0$.

plane completely. We analyze the conditions for stability of different micelle shapes (Figure 13): disk-like micelles (a), stripes (elongated micelles or holes of elongated shape in the bilayer) (b), and "inverse" circular micelles (c), in which case the surface is covered by an all-over bilayer with a few circular pores in it.

Let macromolecules consisting of $N$ amphiphilic monomer units are grafted to a plane surface with the distance $d$ between grafting points, so that $d^2$ is the surface area per macromolecule. The monomer unit volume is equal to $2\upsilon$, the statistical segment length between neighboring $A$ groups in the main chain is equal to $a$. We assume that "bodies" of all micelles constitute a bilayer of constant thickness $h$. The surface is completely covered by the bilayer, if the distance between grafting points is less than the critical value $d_0$,

$$d_0 = \sqrt{2N\upsilon/h}, \tag{9}$$

where $d_0^2$ is the surface area covered by one macromolecule completely included into the bilayer.

In the scaling theory, a single energetic parameter $\varepsilon_b$ is introduced, which denotes the free energy per monomer unit incorporated into the bilayer ($\varepsilon_b < 0$). This free energy includes both the conformational energy penalty due to the compact packing of macromolecule in the bilayer and the energy of its interactions with neighboring units, so that $\varepsilon_b$ is approximately proportional to the characteristic interaction energy of $B$ beads, $\varepsilon_{BB}$. Let $M$ be the aggregation number, i.e., the number of macromolecules per disk-like micelle for the case (a), per part of a stripe of length $d$ for the case (b), and per inverse micelle in the case (c) (Figure 13).

The surface area per micelle is $Md^2$ and the area directly covered by the bilayer is $S_b < Md^2$ (Figure 13). Some macromolecules are fully incorporated into the micelle, their number $M_b$ is assumed to be equal to $M_b = S_b/d^2$, which is approximately valid for quite large values of $M_b$. The other $M - M_b$ macromolecules are incorporated into the micelle only partially, and $q$ denotes the mean fraction of the incorporated monomer units of such macromolecules. The volume of the bilayer (micelle's body) is equal to

$$S_b h = M_b d^2 h = (M_b + (M - M_b)q)2N\upsilon. \tag{10}$$

Macromolecule parts that do not belong to the bilayer (legs) contain $(1 - q)N$ monomer units and they are stretched with the force $f = |\varepsilon_b|/a$. Within the Gaussian chain model, the stretching force can be related to the mean leg size $L_{leg}$,

$$f = k_B T \frac{3L_{leg}}{N(1-q)a^2} = \frac{|\varepsilon_b|}{a}, \tag{11}$$

where $k_B$ is the Boltzmann constant, $T$ is the thermodynamic temperature. The leg size is averaged over the free surface area at the given micelle size $D$ under the assumption of uniform distribution of grafting points. For disk-like micelles, the integration is performed over the square with side length

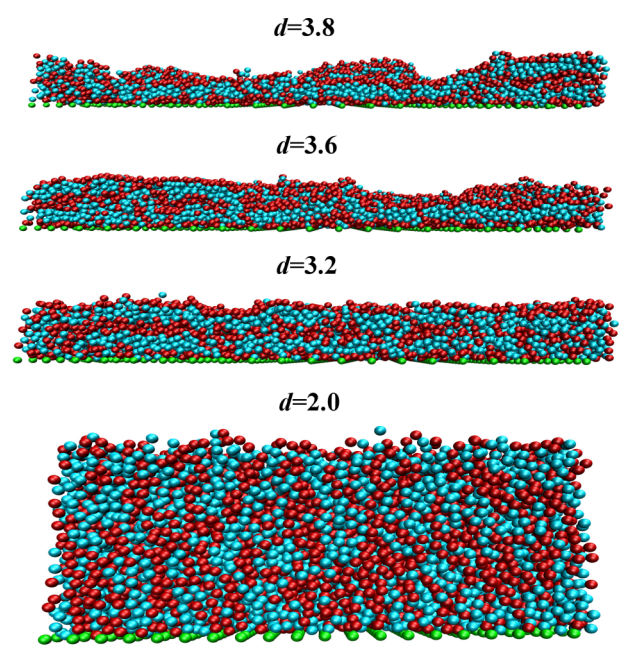


FIG. 12. Side view of simulation cells for different values of $d < d_0$.

This article is copyrighted as indicated in the article. Reuse of AIP content is subject to the terms at: http://scitation.aip.org/termsconditions. Downloaded to IP: 93.180.55.215 On: Thu, 28 May 2015 10:56:03

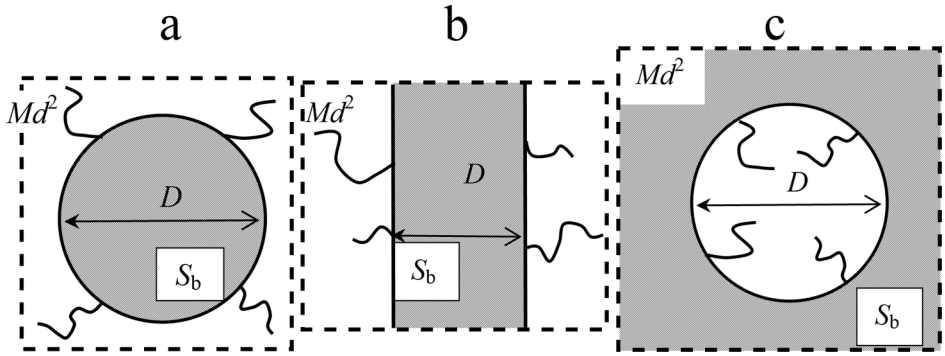


FIG. 13. Different types of bilayer micelles: (a) a disk-like micelle ("spider") of diameter $D$, (b) a stripe of thickness $D$, (c) an "inverse" micelle of diameter $D$.

$\sqrt{M}d$ having the cut circle of diameter $D$:[50]

$$L_{leg(a)} = \frac{1}{(M - M_b)d^2}\left(\int_{D/2}^{d\sqrt{M/2}} dr\, 2\pi r\left(r - \frac{D}{2}\right) - 8\int_{d\sqrt{M}/2}^{d\sqrt{M/2}} dr\, r\left(r - \frac{D}{2}\right)\arccos\frac{d\sqrt{M}}{2r}\right)$$
$$= \frac{d}{M - M_b}\left(\frac{1}{6}\left(\sqrt{2} + \ln(1 + \sqrt{2})\right)M^{3/2} - M\sqrt{\frac{M_b}{\pi}} + \frac{1}{3}\sqrt{\frac{M_b^3}{\pi}}\right), \quad (12)$$

where the area $M_b d^2 = \pi D^2/4$.

For stripes,

$$L_{leg(b)} = \frac{d}{4}(M - M_b). \quad (13)$$

For "inverse" micelles of the area $(M - M_b)d^2 = \pi D^2/4$,

$$L_{leg(c)} = \frac{4}{\pi D^2}\int_0^{D/2} dr\, 2\pi r\left(\frac{D}{2} - r\right) = \frac{D}{6}. \quad (14)$$

For any chosen structure type (a, b, or c), the Eqs. (9)–(14) allow calculating the number of macromolecules $M_b$ and the fraction $q$ at the given area per micelle, $Md^2$. For quite large distances between grafting points, when disk-like micelles exist but cover only a small fraction of the surface ($M_b/M \ll 1$, $q \ll 1$), a leg of the mean size $L_{leg} \approx \sqrt{M}d/3$ is stretched approximately with the force $k_B T\frac{3L_{leg}}{Na^2} \approx \frac{|\varepsilon_b|}{a}$, then $M \approx \left(\frac{\varepsilon_b N a}{k_B T d}\right)^2$.

The free energy per micelle consists of the energy of the micelle body, $F_b$, energy of the boundary line, $F_{line}$, which is analogous to the interfacial free energy for usual bulk micelles, and the conformational energy of stretched legs, $F_{leg}$,

$$F = F_b + F_{line} + F_{leg}. \quad (15)$$

The bilayer free energy is proportional to the number of monomer units in a micelle body $N_b = S_b h/(2\upsilon)$,

$$F_b = N_b\varepsilon_b = M_b\varepsilon_b\frac{d^2 h}{2\upsilon}. \quad (16)$$

The free energy of the boundary line

$$F_{line} = |\varepsilon_b|\, L_{line}/l_{m.u.}, \quad (17)$$

where the free energy of a monomer unit at the boundary line is assumed to be a half of that for a monomer unit inside the micelle, whereas the number of monomer units at the bilayer boundary is equal to $2L_{line}/l_{m.u.}$; the boundary length per monomer unit $l_{m.u.}$ is related to the monomer volume and bilayer thickness by $l_{m.u.} = (4\upsilon/h)^{1/2}$. For disk-like micelles and "inverse" micelles, $L_{line} = \pi D$, where $\pi D^2/4 = M_b d^2$ and $\pi D^2/4 = (M - M_b)d^2$ respectively; for stripes, $L_{line} = 2d$.

The free energy of leg stretching

$$F_{leg} = k_B T(M - M_b)\frac{3}{2}\frac{L_{leg}^2}{(1 - q)Na^2} = (M - M_b)\,|\varepsilon_b|\,\frac{L_{leg}}{2a}. \quad (18)$$

The Eqs. (10)–(18) are valid for quite large values of $M_b$ and $M - M_b$ and they are used in our numerical calculations for $M \geq 3$. The cases of micelles and stripes with small aggregation numbers $M = 1$ and 2 are considered separately. The free energies of a disk-like micelle $F_{1(a)}$ and stripe part $F_{1(b)}$ of length $d$ formed by a single macromolecule ($M = 1$) are equal to

$$F_{1(a)} = -N\varepsilon_b + |\varepsilon_b|\pi D_1/l_{m.u.},$$
$$F_{1(b)} = -N\varepsilon_b + 2|\varepsilon_b|d/l_{m.u.}, \quad (19)$$

respectively, where $2N\upsilon = h\pi D_1^2/4$, $D_1$ is the micelle diameter. Those micelles do not touch each other if $D_1 < d$. Stripes do not merge if $d > d_0$.

In the case $M = 2$, the center of a disk-like micelle or stripe is situated between two grafting points. The volume of a micelle or considered part of the stripe is equal to $4N\upsilon q_2 = h\pi D_2^2/4$ and $4N\upsilon q_2 = hD_2 d$, respectively, $q_2$ is the fraction of monomer units incorporated into the bilayer at $M = 2$, $D_2$ is the disk-like micelle diameter or stripe thickness. Disk-like micelles can exist (do not merge) if $D_2 < d$, then $L_{leg(a)} = (d - D_2)/2$; stripes can exist if $d > d_0$ with $q_2 < 1$, $L_{leg(b)} = (d - D_2)/2$ at $D_2 < d$ and with $q_2 = 1$, $L_{leg(b)} = 0$ at $D_2 > d$. The free energy of a disk-like micelle $F_{2(a)}$ and stripe part $F_{2(a)}$ are equal to

$$F_{2(a)} = -2N\varepsilon_b q_2 + |\varepsilon_b|\pi D_2/l_{m.u.} + |\varepsilon_b|L_{leg(a)}/a,$$
$$F_{2(b)} = -2N\varepsilon_b q_2 + 2|\varepsilon_b|d/l_{m.u.} + |\varepsilon_b|L_{leg(b)}/a, \quad (20)$$

respectively.

This article is copyrighted as indicated in the article. Reuse of AIP content is subject to the terms at: http://scitation.aip.org/termsconditions. Downloaded to IP: 93.180.55.215 On: Thu, 28 May 2015 10:56:03

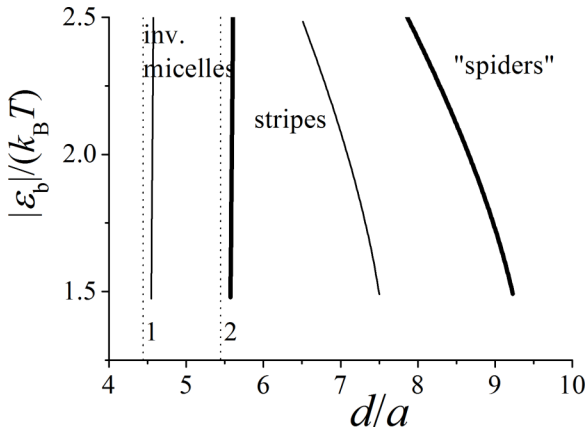


FIG. 14. Diagram of micelle shapes at $d > d_0$ (scaling theory) in the coordinates $d$ (the distance between grafting points) and $|\varepsilon_b|$ (the free energy per monomer unit incorporated into the bilayer, $\varepsilon_b \sim \varepsilon_{BB}$). Thin lines describe the transitions at $N = 32$, thick lines at $N = 48$; $L_{max} = 20d$, $h = 4a$, $\upsilon/a^3 = 1.24$. The vertical dashed lines 1 and 2 correspond to the characteristic $d_0$ value at $N = 32$ and $N = 48$, respectively.

The opposite case of a small number of legs $M - M_b$ corresponds to almost complete coverage of the grafting surface by the bilayer. That case may not be described in terms of the scheme ((10)–(18)) as well. Let us consider the free energies of stripes and inverse micelles in the limit $d \to d_0$ (disk-like micelles can not provide almost all-over coverage). Since no arms are finally formed, the free energy is the sum of the bilayer term (16) and line term (17). Then, the minimum of the free energy per macromolecule $F_{min}/M = \varepsilon_b N$ is identically the same both for inverse micelles and stripes at $M \to \infty$.

For the given micelle type, the minimum of the free energy per macromolecule, $F/M$, with respect to the aggregation number $M$ corresponds to a set of the equilibrium parameters of micelles. Comparing the free energies per macromolecule $F/M$ (15), $F_1$ (19), and $F_2/2$ (20) for all considered structures (a, b, and c), the most favorable shape of micelles can be found.

Directly applying the scheme of calculations (10)–(18) at $d \approx d_0$, the formation of extremely wide stripes could be predicted. However, if we assume that the system relaxation takes place at a certain kinetically accessible scale $L_{max}$, the transition from stripes to inverse micelles appears with increasing the grafting density. Graphs below are plotted under the condition that the size of the region per stripe $Md$ and per inverse micelle $\sqrt{M}d$ is less than $L_{max}$ (in calculations $L_{max} = 20d$ as the size of the simulation box).

At the diagram with the axes $d$ and $|\varepsilon_b|$ (Figure 14), the regions are shown, where one of the above-considered micelle shape is most favorable. The parameter values $h = 4a$ and $\upsilon/a^3 = 1.24$ are related to the computer simulations, two chain lengths $N = 32$ and $N = 48$ are used in calculations. The vertical dashed lines mark the values $d_0 \approx 4.45a$ for $N = 32$ and $d_0 \approx 5.46a$ for $N = 48$ found from Eq. (9), which correspond to the complete surface coverage of the bilayer. The increase of $d$ corresponds to the decrease in the grafting density.

The disk-like micelles ("spiders") are formed at low grafting density, stripes (elongated micelles or holes of elongated shape in the bilayer) at moderate grafting density, and inverse micelles are formed for very dense grafting. It is worth to note that the free energies per macromolecule, $F/M$, for stripes and inverse micelles in the region of inverse micelles in the Figure 14 differ less than by $k_BT$, so that stripes and inverse micelles can coexist in that region. That conclusion is supported by the computer simulation (see Figure 6 for $d = 4.6$), where the circular and elongated holes are present simultaneously. A transition from stripes to "spiders" with increasing $|\varepsilon_b|$ (worsening solvent quality, $\varepsilon_b \sim \varepsilon_{BB}$) is also supported by the simulation results: breaking one elongated micelle in the middle of Fig. 2(c) in two smaller micelles (Figure 2(d)) can be observed. Large values of $|\varepsilon_b|$ are not considered here since they correspond to very high stretching of legs that may not be described in terms of the Gaussian chain model (the value $|\varepsilon_b|/(k_BT) = 3$ means that legs are fully straightened). The minimum of the free energy $F$ given by Eq. (15) with respect to the aggregation number $M$ is not sharp, therefore, micelles of the same shape with different but close aggregation numbers can coexist, as well as micelles of different shapes in the vicinity of borderlines.

The dependences of the aggregation number $M$ and fraction of the covered surface area $f_S$ on the distance $d$ between grafting points are plotted in Figures 15 and 16. With increasing $d$ (decreasing the grafting density), the aggregation number decreases for micelles of any type taken separately. A stepwise decrease of the aggregation number at $d/a = 4.55$-$4.6$ for $N = 32$ and $d/a \approx 5.6$ for $N = 48$ corresponds to the transition from inverse micelles to stripes (pay attention to the breaks in the vertical axis). The aggregation number $M$ characterizing the ensemble of micelles in computer simulations changes smoothly with $d$,

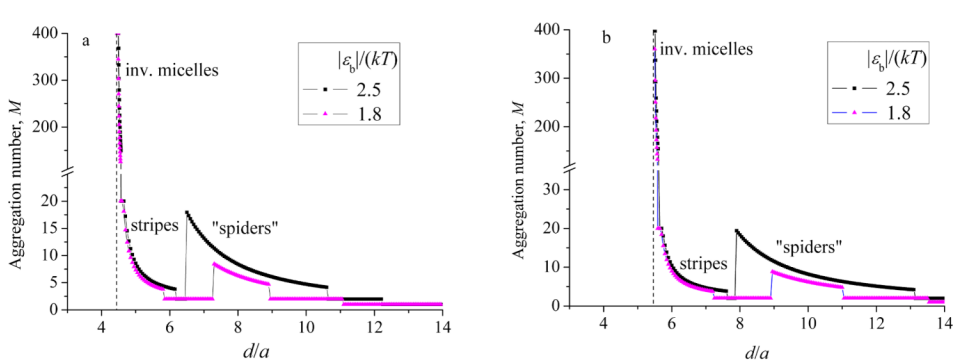


FIG. 15. The aggregation number $M$ vs. the distance $d$ between grafting points calculated for different values of the free energy per monomer unit incorporated into the bilayer $\varepsilon_b$ and for different values of the chain length: $N = 32$ (a), $N = 48$ (b); $L_{max} = 20d$, $h = 4a$, $\upsilon/a^3 = 1.24$.

This article is copyrighted as indicated in the article. Reuse of AIP content is subject to the terms at: http://scitation.aip.org/termsconditions. Downloaded to IP: 93.180.55.215 On: Thu, 28 May 2015 10:56:03

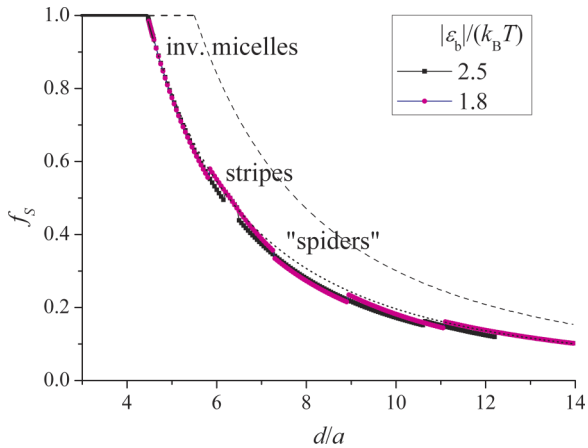


FIG. 16. The fraction of the covered surface area $f_S$ vs. the distance $d$ between grafting points for different values of the free energy per monomer unit incorporated into the bilayer $\varepsilon_b$; $L_{max} = 20d$, $h = 4a$, $\upsilon/a^3 = 1.24$. The dotted and dashed lines correspond to the complete incorporation of monomer units into the bilayer (without legs, $K_{gr} = 1$) $f_S = 2N\upsilon/(d^2h)$ for $N = 32$ and $N = 48$, respectively.

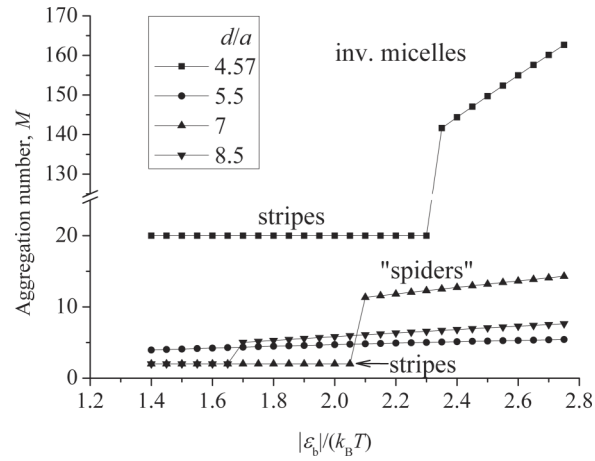


FIG. 17. The aggregation number $M$ vs. the free energy per monomer unit incorporated into the bilayer $\varepsilon_b$ for different values of the distance $d$ between grafting points; $N = 32$, $L_{max} = 20d$, $h = 4a$, $\upsilon/a^3 = 1.24$.

whereas the corresponding curves in theory have steps at the curves. Those steps between stripes and other structure types are due to the calculation of the number of macromolecules per part of an infinite stripe of length $d$, whereas the elongated micelles are finite in the computer simulations.

The aggregation number of stripes (the number of macromolecules per part of a stripe of length $d$) decreases to 2 and then increases at the transition to "spiders". Small steps down to the values $M = 1$ and 2 for "spiders" and stripes are due to the separate calculations of the free energy at small aggregation numbers ($M = 1$ and 2).

Let us compare the numerical data for the aggregation number $M$ (Fig. 15(a)) and the fraction of the covered surface $f_S$ (Fig. 16) at $N = 32$ with those in simulations (Fig. 7). Note that they are plotted for the energetic parameters $\varepsilon_b$ in theory and parameter $\chi$ in simulations that cannot be related directly. The value $\chi = 5.7$ corresponds visually to quite strong stretching of "spider" legs that cannot be treated in terms of the present theory. The numerical values of the aggregation numbers for "spiders" at $|\varepsilon_b|/kT = 2.5$ in Fig. 15(a) are about 1.5 times less that those in computer simulations (Fig. 7(a)), compared at the same ratio $d/d_0$. Since the aggregation number grows with $|\varepsilon_b|$ (Fig. 15(a)), the higher values can be expected for the solvent quality corresponding to $\chi = 5.7$. Hence, we infer that the simulation and theoretical data agree with each other. The difference in the fraction of covered surface is even smaller: $f_S = 0.5$ at $d/d_0 = 1.45$ in the simulations and at $d/d_0 = 1.37$ in the theory.

The fraction of the covered surface area was calculated as $f_S = M_b/M$ if corresponding value of the aggregation number $M \geq 3$ (Figure 17). At $M = 1$ and 2, we used $f_S = D_1/d$ and $D_2/(2d)$ for stripes and $f_S = \pi D_1^2/(4d^2)$ and $\pi D_2^2/(8d^2)$ for "spiders", respectively. The curves with markers describing $f_S$ at $|\varepsilon_b|/(k_BT) = 1.8$ and 2.5 are very close to the dotted curve that corresponds to the complete incorporation of monomer units into the bilayer (for the case of macromolecules not forming legs, $K_{gr} = 1$). The maximum difference between those curves is attained for disk-like micelles with high aggregation numbers in the scaling model and for the fraction $K_{gr}$ minimum in the computer simulations (Figure 8).

Increasing the attraction energy between side groups of the monomer units, i.e., the value of $|\varepsilon_b|$, leads to the aggregation number growth; the large steps of the curves for $d/a = 4.57$ and $d/a = 7$ correspond to the changes of micelle types. The curve for $d/a = 5.5$ corresponds to stripes only and that for $d/a = 8.5$ to "spiders" only.

## V. CONCLUSIONS

We have studied the self-organization of grafted layers of macromolecules composed of monomer units each comprising a hydrophobic side-group and a hydrophilic group in the backbone. It was shown that the attractive interaction between side-groups leads to the formation of structured micelles due to the effective separation between hydrophobic and hydrophilic groups. Three different regimes have been distinguished in the dependence on the grafting density. In case of low grafting density $d \geq d_0 \sim \sqrt{N}$, the micelles are ultrathin, their thickness is about the double size of monomer unit and their shape change with increase of grafting density as single globule—circular micelles—prolonged micelles—inverse micelles—homogeneous bilayer. In the interval $d^* < d < d_0$ ($d^* = d_0/\sqrt{2}$), the micelles are formed above the thin monomer bilayer. With increase of grafting density, the shape of such over-built micelles is changed consequently as circular micelles—lamellas—inverse micelles—double bilayer. At high grafting density with $d < d^*$, the grafted macromolecules form compacted layer without visible parallel to grafting surface segregation of monomers.

Thus, we first have found that the change of solvent quality could lead to transition from swollen polymer brush to ultra-thin film spreading over the grafting surface and having specific layering order. The effects could be observed both in described-above case of amphiphilic monomer units consisting of solvophobic and solvophilic groups and in the case of amphiphilic comb-like copolymers.[51–54] This fact could be prospective for creation of new types of smart responsive surfaces.

This article is copyrighted as indicated in the article. Reuse of AIP content is subject to the terms at: http://scitation.aip.org/termsconditions. Downloaded to IP: 93.180.55.215 On: Thu, 28 May 2015 10:56:03

## ACKNOWLEDGMENTS

This research was supported financially by Russian Science Foundation (Project No. 14-13-00745) and carried out in A.N. Nesmeyanov Institute of Organoelement Compounds of Russian Academy of Sciences.

[1]H. Kanazawa, Y. Matsushima, and T. Okano, TrAC, Trends Anal. Chem. **17**, 435 (1998).
[2]A. Kumar, A. Srivastava, I. Yu. Galaev, and B. Mattiasson, Prog. Polym. Sci. **32**, 1205 (2007).
[3]A. Halperin, M. Tirrell, and T. P. Lodge, Adv. Polym. Sci. **100**, 31–71 (1992).
[4]K. Binder and A. Milchev, J. Polym. Sci., Part B: Polym. Phys. **50**, 1515 (2012).
[5]S. K. Pattanayek, T. T. Pham, and G. G. Pereira, J. Chem. Phys. **122**, 214908 (2005).
[6]V. Koutsos, E. W. van der Vegte, and G. Hadziioannou, Macromolecules **32**, 1233 (1999).
[7]B. Zhao, W. J. Brittain, W. Zhou, and S. Z. D. Cheng, J. Am. Chem. Soc. **122**, 2407 (2000).
[8]W. J. Brittain, S. G. Boyes, A. M. Granville, M. Baum, B. K. Mirous, B. Akgun, B. Zhao, C. Blickle, and M. D. Foster, Adv. Polym. Sci. **198**, 125 (2006).
[9]X. Gao, W. Feng, S. Zhu, H. Sheardown, and J. L. Brash, Langmuir **24**, 8303 (2008).
[10]P. Yang and Y. Han, Macromol. Rapid Commun. **30**, 1509 (2009).
[11]S. B. Rahane, J. A. Floyd, A. T. Metters, and S. M. Kilbey II, Adv. Funct. Mater. **18**, 1232 (2008).
[12]K. Yu, H. Wang, L. Xue, and Y. Han, Langmuir **23**, 1443 (2007).
[13]K. Yu and Y. Han, Soft Matter **5**, 759 (2009).
[14]B. M. D. O'Driscoll, G. H. Griffiths, M. W. Matsen, S. Perrier, V. Ladmiral, and I. W. Hamley, Macromolecules **43**, 8177 (2010).
[15]B. M. D. O'Driscoll, G. E. Newby, and I. W. Hamley, Polym. Chem. **2**, 619 (2011).
[16]E. B. Zhulina, C. Singh, and A. C. Balazs, Macromolecules **29**, 6338 (1996).
[17]E. B. Zhulina, C. Singh, and A. C. Balazs, Macromolecules **29**, 8254 (1996).
[18]D. Meng and Q. Wang, J. Chem. Phys. **130**, 134904 (2009).
[19]Y. Yin, P. Sun, B. Li, T. Chen, Q. Jin, D. Ding, and A.-C. Shi, Macromolecules **40**, 5161 (2007).
[20]M. W. Matsen and G. H. Griffiths, Eur. Phys. J. E **29**, 219 (2009).
[21]O. A. Guskova and C. Seidel, Macromolecules **44**, 671 (2011).
[22]G. Brown, A. Chakrabarti, and J. F. Marko, Macromolecules **28**, 7817 (1996).
[23]P. G. Ferreira and L. Leibler, J. Chem. Phys. **105**, 9362 (1996).
[24]M. K. Glagolev, V. V. Vasilevskaya, and A. R. Khokhlov, Polym. Sci., Ser. A **54**, 767 (2012).
[25]A. A. Rudov, P. G. Khalatur, and I. I. Potemkin, Macromolecules **45**, 4870 (2012).
[26]E. N. Govorun and D. E. Larin, Polym. Sci., Ser. A **56**, 770 (2014).
[27]A. Goldar and J.-L. Sikorav, Eur. Phys. E **14**, 211 (2004).
[28]I. M. Okhapkin, E. E. Makhaeva, and A. R. Khokhlov, Colloid Polym. Sci. **284**, 117 (2005).
[29]I. M. Okhapkin, A. A. Askadskii, V. A. Markov, E. E. Makhaeva, and A. R. Khokhlov, Colloid Polym. Sci. **284**, 575 (2006).
[30]V. V. Vasilevskaya, P. G. Khalatur, and A. R. Khokhlov, Macromolecules **36**, 10103 (2003).
[31]V. V. Vasilevskaya, A. A. Klochkov, A. A. Lazutin, P. G. Khalatur, and A. R. Khokhlov, Macromolecules **37**, 5444 (2004).
[32]V. V. Vasilevskaya, V. A. Markov, P. G. Khalatur, and A. R. Khokhlov, J. Chem. Phys. **124**, 144914 (2006).
[33]A. A. Glagoleva, V. V. Vasilevskaya, K. Yoshikawa, and A. R. Khokhlov, J. Chem. Phys. **139**, 244901 (2013).
[34]V. V. Vasilevskaya and V. A. Ermilov, Polym. Sci., Ser. A **53**, 846 (2011).
[35]A. K. Tucker and M. J. Stevens, J. Chem. Phys. **139**, 104907 (2013).
[36]V. V. Vasilevskaya, V. A. Markov, G. ten Brinke, and A. R. Khokhlov, Macromolecules **41**, 7722 (2008).
[37]M. K. Glagolev, V. V. Vasilevskaya, and A. R. Khokhlov, J. Chem. Phys. **137**, 084901 (2012).
[38]A. R. Khokhlov and P. G. Khalatur, Chem. Phys. Lett. **461**, 58 (2008).
[39]A. A. Glagoleva, V. V. Vasilevskaya, and A. R. Khokhlov, Polym. Sci., Ser. A **52**, 182 (2010).
[40]A. A. Glagoleva, V. V. Vasilevskaya, and I. Ya. Erukhimovich, Macromol. Theory Simul. **22**, 31 (2013).
[41]A. S. Ushakova, E. N. Govorun, and A. R. Khokhlov, J. Phys.: Condens. Matter **18**, 915 (2006).
[42]A. V. Subbotin and A. N. Semenov, Polym. Sci., Ser. C **54**, 36 (2012).
[43]S. J. Plimpton, J. Comput. Phys. **117**, 1 (1995).
[44]V. Sadovnichy, A. Tikhonravov, Vl. Voevodin, and V. Opanasenko, "'Lomonosov': Supercomputing at Moscow state university," in *Contemporary High Performance Computing: From Petascale Toward Exascale*, edited by J. S. Vetter (Chapman & Hall/CRC Computational Science, CRC Press, Boca Raton, USA, 2013), pp. 283–307.
[45]P. J. Flory, *Principles of Polymer Chemistry* (Cornell University Press, Ithaca, NY, 1953).
[46]A. Yu. Grosberg and A. R. Khokhlov, *Statistical Physics of Macromolecules* (AIP Press, New York, 1994).
[47]K. Kremer and G. S. Grest, J. Chem. Phys. **92**, 5057 (1990).
[48]F. F. Abraham and Y. Singh, J. Chem. Phys. **67**, 2384 (1977).
[49]T. Schneider and E. Stoll, Phys. Rev. B **17**, 1302 (1978).
[50]H. B. Dwight, *Tables of Integrals and Other Mathematical Data*, 4th ed. (The Macmillan Co., New York, 1961).
[51]S. Minko, J. Macromol. Sci. C, Polym. Rev. **46**, 397 (2006).
[52]A. Synytska, E. Svetushkina, D. Martina, C. Bellmann, F. Simon, L. Ionov, M. Stamm, and C. Creton, Langmuir **28**, 16444 (2012).
[53]M. Lillethorup, K. Shimizu, N. Plumere, S. U. Pedersen, and K. Daasbjerg, Macromolecules **47**, 5081 (2014).
[54]A. Synytska, E. Biehlig, and L. Ionov, Macromolecules **47**, 8377 (2014).

This article is copyrighted as indicated in the article. Reuse of AIP content is subject to the terms at: http://scitation.aip.org/termsconditions. Downloaded to IP: 93.180.55.215 On: Thu, 28 May 2015 10:56:03